



**Nucleation and Growth of Blue Phase Liquid Crystals on Chemically-Patterned Surfaces: A Surface Anchoring Assisted Blue Phase Correlation Length**

Journal:	<i>Molecular Systems Design &amp; Engineering</i>
Manuscript ID	ME-ART-05-2021-000044.R1
Article Type:	Paper
Date Submitted by the Author:	25-May-2021
Complete List of Authors:	Li, Xiao; University of North Texas, Material Science and Engineering Park, Kangho; The University of Chicago Guzmán, Orlando; The University of Chicago Martinez-Gonzalez, Jose Adrian; Universidad Autonoma de San Luis Potosi, Facultad de Ciencias Dolan, James; University of Cambridge, Electrical Engineering de Pablo, Juan; Liew Family Professor of Molecular Theory and Simulation, Institute for Molecular Engineering Nealey, Paul; Institute for Molecular Engineering , University of Chicago

SCHOLARONE™  
Manuscripts

## **Nucleation and Growth of Blue Phase Liquid Crystals on Chemically-Patterned Surfaces: A Surface Anchoring Assisted Blue Phase Correlation Length**

*Xiao Li<sup>1\*</sup>, Kangho Park<sup>2,3</sup>, Orlando. Guzmán<sup>2,4</sup>, José A. Martínez-González<sup>5</sup>, James A Dolan<sup>6</sup>, Juan J. de Pablo<sup>2,7</sup> and Paul F. Nealey<sup>2,7\*</sup>*

### **Design, System, Application Statement**

Blue phases (BPs) are chiral liquid crystals with a regular lattice of topological defects. Through molecular self-assembly, BPs' unique soft-matter symmetries provide materials with many excellent properties that are different from conventional liquid crystals. Especially, chemically-patterned surfaces have been developed to direct the self-assembly of BPs into perfect single-crystals with desired lattice orientation, thereby further benefitting the design of photonics and smart electro-optical devices. However, the correlation length of BPs — defined as the distance over which the same BP-lattice orientation is maintained, an essential design parameter— has remained unrevealed until now. Here, nanoscale chemical-pattern design of alternate planar and homeotropic anchoring stripes allows a systematic study of the growth of BPs outside the patterned area along different kinetic pathways, as well as the time evolution of the correlation length. New understanding of the correlation length can be used to guide a rational design of macroscopic single-crystals of BPs reliant on reduced patterned surfaces, which opens exciting opportunities to apply this intriguing class of materials for exploration and development of new BPLC-based functionalities and devices for advanced optical devices or soft material design.

# **Nucleation and Growth of Blue Phase Liquid Crystals on Chemically-Patterned Surfaces: A Surface Anchoring Assisted Blue Phase Correlation Length**

*Xiao Li<sup>1\*</sup>, Kangho Park<sup>2,3</sup>, Orlando Guzmán<sup>2,4</sup>, José A. Martínez-González<sup>5</sup>, James A Dolan<sup>6</sup>, Juan J. de Pablo<sup>2,7</sup> and Paul F. Nealey<sup>2,7\*</sup>*

<sup>1</sup>Department of Materials Science and Engineering, University of North Texas, Denton, TX 76203, USA.

<sup>2</sup>Pritzker School of Molecular Engineering, The University of Chicago, Chicago, IL 60637, Unites States.

<sup>3</sup>Samsung Electronics Co., Ltd, 1 Samsungjeonja-ro, Hwasung-City, Gyeonggi-Do, 18448, Republic of Korea.

<sup>4</sup>Departamento de Física, Universidad Autónoma Metropolitana Iztapalapa, Av. San Rafael Atlixco 186, Ciudad de México 09340, México.

<sup>5</sup>Facultad de Ciencias, Universidad Autónoma de San Luis Potosí, Av. Parque Chapultepec 1570, San Luis Potosí 78210, SLP, México

<sup>6</sup>Department of Chemistry, University of Cambridge, Lensfield Road, Cambridge, CB2 1EW, UK

<sup>7</sup>Center for Molecular Engineering, Argonne National Laboratory, Lemont, IL 60439, United States.

\*Correspondence to: Xiao.Li@unt.edu; nealey@uchicago.edu

Keywords: blue phase liquid crystal, directed self-assembly, chemical pattern, crystal growth, correlation length

## Abstract

In condensed matter, the correlation length is an essential parameter which describes the distance over which a material maintains its structural properties. In liquid crystals, for orientational order parameter this characteristic length is of the order of nanometer, while in solid crystals it can extend to macroscopic length scales. Here, we report the measurement of the correlation length, or persistence length, of the crystallographic orientation of blue phases (BPs)—chiral liquid crystals with long-range 3D-crystalline structures and submicron-sized lattice-parameters. These materials exhibit phase transformations that have been identified as the liquid analog of crystal-crystal martensitic transformations. In this work, we use liquid epitaxial growth to achieve spontaneous BP-crystal nucleation and subsequent growth. Specifically, we design patterned substrates made of a binary array of regions with different liquid crystal anchoring, which facilitate a uniform nucleation and growth of BP-crystals with (100)-lattice orientation and a simple cubic symmetry. Our results indicate that this simple cubic BP, the so-called blue phase II (BPII), forms first on the patterned surface, thereby propagating the growth of domains in directions parallel or perpendicular to the patterned regions. These results are used to understand the emergence of a surface anchoring assisted BPII-correlation length, taken as the distance over which the BP preserves its lattice orientation, as a function of time and pattern characteristics. We found that BPII single crystals can be achieved on patterned regions whose lateral dimensions are equal to or larger than 10  $\mu\text{m}$ , consistent with our measurements of the BPII-correlation length. This newly acquired understanding of the role of surfaces on the formation of BPs is then used to design processes that permit formation of macroscopically large mono-domain, single-crystal BPs by relying on significantly reduced patterned areas (only part of the area is patterned), a feature that could benefit the applications of this intriguing class of materials.

## Introduction

In anticipated future applications of both nanotechnology in general, and molecular engineering in particular, it is extremely important to exert precise control over the constituent components of the system under study. In this context, the analysis and design of strategies to achieve directed molecular self-assembly have attracted significant attention. In liquid crystal research, directed self-assembly approaches are particularly challenging since liquid crystals

are extraordinarily sensitive to external stimuli. Here we rely on nanoscale chemical pattern design and the liquid analog of epitaxial growth to bias the crystal nucleation of the so-called blue phases (BPs) in liquid crystals. BPs are thermodynamically stable chiral liquid crystal states that occur within a narrow range of temperature between the cholesteric (Chol) and the isotropic (I) phases. In BPs, molecules orient and organize locally in such a manner as to produce structures known as double twist cylinders (DTCs), which balance long-range elastic distortions with short-range interfacial contributions to the free energy. These DTCs can then arrange themselves into a body centered cubic (BCC) structure to form the so-called blue phase I (BPI). Alternatively, they can form a simple cubic (SC) structure, which is referred to as the blue phase II (BPII). In both cases, the lattice parameters are in the sub-micron scale, and the DTC array is inter-dispersed by a well-defined network of liquid-crystalline line defects<sup>1-4</sup> (Fig. 1a). In some cases, the DTCs adopt amorphous configurations, leading to formation of the blue phase III (BPIII)<sup>5-6</sup>. BPs exhibit Bragg reflection of visible light and fast electro-optical switching, with sub-millisecond response times, making them highly attractive for photonic<sup>7-9</sup> and electro-optical device applications<sup>10-14</sup>. In spite of these advantages, however, the practical use of BPs has been limited by their narrow range of thermal stability, and by the fact that BPs usually grow as polycrystalline structures with an abundance of grain boundaries and different grain orientations, both of which limit ultimate device performance.

Among the different approaches that have been explored to reduce poly-domain formation over large areas<sup>15-20</sup>, the use of chemically-patterned surfaces<sup>21</sup> has been shown to be particularly effective in directing the self-assembly of the DTCs into homogeneous single-crystal BPs that adopt a prescribed lattice orientation. More specifically, controlled BP-crystal nucleation and growth are achieved by designing chemical patterns that impose, with nanoscale precision, planar or homeotropic molecular alignments at a surface. The symmetry and dimensions of the chemical pattern dictates the lattice orientation of the BP crystal that is formed<sup>22</sup>. Once the BP-single crystal is produced on the patterned surface, it can propagate into surrounding, un-patterned regions<sup>23</sup>. In this work, such un-patterned regions exhibit uniform and homeotropic anchoring. The fact that the BP-crystal grows outside the patterned area can be utilized to significantly reduce the total pattern area while still maintaining a macroscopically large single crystal. This necessitates a clear understanding of the growth characteristics of BPs along different directions, parallel or perpendicular to the pattern direction, such that disparate

domains could ultimately connect in a well-defined manner and form a single-crystal BP monodomain.

The main purpose of this work is to develop the understanding of BP-single crystal's propagation by characterizing the correlation length of the BP. In liquid crystal research, the correlation length is commonly associated with the scalar order parameter, or the distance over which directors maintain the same orientation when an external field is applied in some limited region of space<sup>24-25</sup>. Here, the correlation length is defined as the distance over which the same BP-lattice orientation is maintained<sup>15,26-28</sup>. The design patterned characteristics allows us to track the growth of BPs outside the patterned area along different kinetic pathways<sup>29</sup>, as well as change of the correlation length with time.

The patterns considered here consist of alternating planar and homeotropic anchoring stripes that facilitate uniform and fast nucleation and growth of single BPII-crystals with (100)-lattice orientation out-of-plane ( $\text{BPII}_{(100)}$ ). The un-patterned surfaces exhibit uniform homeotropic anchoring, leading to growth of polycrystalline BPII dominated by platelets with (111)-lattice orientation out-of-plane ( $\text{BPII}_{(111)}$ ). The correlation length is studied during a quenching process starting from the isotropic phase. The patterned stripes are created in rectangular regions of various geometries, referred to as "long" and "short". All patterned regions have the same area and are patterned with the same chemical stripes; the difference is that in the "long" regions the long axis of the chemical stripes is parallel to the long axis of the rectangular patterned area, while in the "short" regions the long axis of the chemical stripes is perpendicular to the long axis of the rectangular patterned area, as depicted in Figures 1b and 2c. We first determine the minimum value of the width,  $w_p$ , of the rectangular areas for which a  $\text{BPII}_{(100)}$  single crystal is formed on the chemically-patterned area and which propagates onto the neighboring uniform homeotropic region (i.e. a non-zero correlation length). After the minimum widths of the long- and short-type regions are determined, we perform heating and cooling processes to analyze how the  $\text{BPII}_{(100)}$  crystal grows along the directions parallel and perpendicular to the chemical stripes. Finally, we demonstrate that it is possible to produce macroscopic BPII crystals by patterning only a fraction of the entire substrate.

## Results and Discussion

In this work, the chiral liquid crystal (ChLC) material consists of MLC2142 LC mixed with 36

wt% of the chiral dopant 4-(1-methylheptyloxycarbonyl)phenyl-4-hexyloxybenzoate (S811). For this chiral concentration, BPs can be obtained by a heating process from room temperature (0.2 °C / min), yielding the following transition temperatures:  $T_{\text{Chol-BPI}} = 39.9 \pm 0.05^\circ\text{C}$ ,  $T_{\text{BPI-BPII}} = 40.7 \pm 0.05^\circ\text{C}$ , and  $T_{\text{BPII-Iso}} = 42.9 \pm 0.05^\circ\text{C}$ . The unit-cell sizes of the BPs correspond to  $a = 255$  nm for BPI and  $a = 150$  nm for BPII, where  $a$  is the lattice parameter<sup>21</sup>. According to Braggs' law, the wavelength of light reflected from the  $(hkl)$  plane is given by  $\lambda_{(hkl)} = 2na / \sqrt{h^2 + k^2 + l^2}$ , where  $n$  is the refraction index. BPI<sub>(110)</sub> reflects green light with  $\lambda_{(110)} = 540$  nm, and BPII<sub>(100)</sub> reflects blue light with  $\lambda_{(100)} = 450$  nm. The reflection of light from other planes is not in the visible range: for example, (110) and (111) planes of BPII reflect light with  $\lambda_{(110)} = 318$  nm and  $\lambda_{(111)} = 260$  nm, respectively. The chemical patterns are fabricated according to our previously published work<sup>30</sup>. The patterned surface consists of an array of alternating planar and homeotropic anchoring stripes, each 75 nm wide. The ChLC was confined within a hybrid cell that consists of an octadecyltrichlorosilane (OTS)-coated glass top surface and the chemically-patterned silicon bottom surface (substrate) with a 3.5 μm gap. The ChLC was injected into the cell by capillary action above the isotropic temperature. Once the BPII is formed on the patterned regions, its blue color comes from the light reflected by the (100)-planes<sup>21</sup>. Micrographs are taken by polarized optical microscopy (POM) and the lattice orientation is confirmed by inspection of the corresponding Kossel diagram.

### Correlation length of BPII on chemically-patterned surface

The two types of rectangular stripe-patterned areas depicted in Figs. 1b and 1c were conceived to partially cover a 440 x 440 μm area. Again,  $w_p$  is the width of such rectangular areas, which are separated from one another by uniform homeotropic regions of width  $w_h$ . Figure 1 shows several SEM images of the chemical patterns; each bright section corresponds to a rectangular patterned area, and the zoomed-in views of these sections show the details of the chemical stripes corresponding to the alternating planar and homeotropic anchoring. Our experimental platform offers the possibility to control, measure, and visualize the dynamics of crystal growth during the thermal processes that lead to formation of a macroscopic BPII<sub>(100)</sub> single-crystal.

An array of rectangular patterned sections of different widths,  $w_p$ , from 3 to 135 μm (see Figs. 2 a-d), was first explored with the purpose of estimating the minimum value of  $w_p$  for which a BPII<sub>(100)</sub> single crystal is formed on the chemically-patterned area. In all cases, the length of

the rectangular areas was kept at 400  $\mu\text{m}$ . The optical microscopy (OM) images of long- and short-type patterned areas are shown in Figs. 2 b-d. The liquid crystal is taken to the BPII temperature by first heating it to the isotropic temperature and then enacting a one-step quench process, maintaining it at 0.2  $^{\circ}\text{C}$  above  $T_{\text{BPI-BPII}}$ . This results in the formation of  $\text{BPII}_{(100)}$  on the patterned surfaces (Fig. 2 e-g), while the uniform homeotropic anchoring background area is mainly occupied by  $\text{BPII}_{(111)}$  monodomains. For the 3 and 5  $\mu\text{m}$  widths, the patterned areas are not sufficiently large to maintain a uniform  $\text{BPII}_{(100)}$ . However, when  $w_p \geq 10 \mu\text{m}$ , the  $\text{BPII}_{(100)}$  grows over the chemically-patterned area and extends into its surroundings. Figures 2 f and h correspond to representative cases for both the long- type and short-type patterned regions. They highlight a distribution of the distance that the  $\text{BPII}_{(100)}$  crystal extends beyond the chemically-patterned area. We identify the average of this distance as the correlation length,  $w_g$ , of BPs assisted by chemically-patterned surfaces.

Figures 2 i-j demonstrate that the correlation length of the  $\text{BPII}_{(100)}$  does not depend on the width of the chemically-patterned areas. We can appreciate from the figure that  $w_g$  is approximately  $11 \pm 1 \mu\text{m}$  and  $7 \pm 1 \mu\text{m}$  for the long and the short-type pattern, respectively. The correlation length is, however, found to be dependent on the crystal growth time. We found that for the long-type pattern,  $w_g$  increases with time and seems to converge to  $\sim 12 \mu\text{m}$ ; for the short-type pattern,  $w_g$  similarly increases and approaches  $\sim 7 \mu\text{m}$ . After 5 minutes (at 40.9 $^{\circ}\text{C}$ ), the  $\text{BPII}_{(100)}$  crystal stops growing. Figure 2k shows several micrographs of the  $\text{BPII}$ -crystal at different times when  $w_p = 10 \mu\text{m}$ , and Fig. 2l shows the time dependence of the correlation length for the long-type and short-type patterned areas. According to the universal growth laws for describing the phase order kinetics<sup>31</sup>,  $L(t) \sim t^n$ , where  $L$  is the correlation length or propagation length of BP,  $t$  is the time and  $n$  is the growth exponent. The time dependence of the correlation length shown in Fig. 2l can be understood as two growth regimes: First, for about the first 300 s, a short-time phase-ordering regime with growth exponents close to  $n=1/2$ ; this is consistent with observations and analysis by Dierking<sup>28</sup>, where a growth exponent  $n=1/2$  was attributed to a very small difference in free energies driving the growth (as that required for specific lattice orientation<sup>22</sup>). In the second regime, after the first 300 s, the size becomes independent of time, keeping almost a constant value within the experimental time frame. Here, the one-step quench depth is  $\Delta T = 2 \text{ }^{\circ}\text{C}$  with a large stable single crystal of BP formed in 60 s<sup>29</sup>. We observe relatively quick growth of nucleus for the short-time process, reaching

equilibrium with a constant value afterwards, which is consistent with previous report<sup>28</sup>. The difference is that the formation of BP single crystal in our setup only takes a few seconds, since the chemically patterned surface can drive the total free energy of the system down by growth. Moreover, the non-pattern-directed BP texture would take much longer time to prepare (usually a few hours or days), and larger super-cooling ( $\Delta T > 2$  °C) may not cause BP formation but only lead to the cholesteric N\* phase<sup>28</sup>. Therefore, the chemically patterned surface stabilized BP with a slightly lower free energy allows a relatively larger quench depth, but still maintains the single crystal and its propagation outside the patterned area. We also found that the correlation length of BPII<sub>(100)</sub> formed on long-type pattern is twice as large as that for the short-type pattern. The above observations indicate that the  $w_p$  value of the chemically-patterned areas needed to form a single-crystal BPII<sub>(100)</sub> is above 10  $\mu\text{m}$ , and that the correlation length is mainly affected by the crystal growth time and the chemical pattern type.

### **BPII crystal nucleation and growth on reduced pattern surface from the isotropic phase**

The nucleation, growth, and formation of a BPII<sub>(100)</sub> crystal are examined during cooling from the isotropic phase. The substrate has a reduced pattern area (i.e. only c. 66% of the total area is patterned), with alternating chemically-patterned and non-patterned regions ( $w_p = 10$   $\mu\text{m}$ ,  $w_h = 5$   $\mu\text{m}$ ). The initial uniform temperature of the isotropic liquid is 42.9°C. Three cooling schemes are considered: (1) a single deep quench,  $\Delta T = 2$ °C, (2) two quench steps, for which each step  $\Delta T = 1$ °C, and (3) a sequence of cooling steps in which temperature is decreased by 0.4 °C per minute. Figure 3 summarizes our results for the three cooling schemes on the long-type chemical pattern. In our hybrid cell, surface mediated nucleation will favor BPII<sub>(100)</sub> formation from the patterned surface and BPII<sub>(111)</sub> formation from the top surface. The material also undergoes natural convection cooling at the top, but the low thermal conductivity and the thickness of the top glass direct the heat flow through the Si-bottom surface<sup>29</sup>. As shown in Figure 3a, based on the deep quench depth, ( $\Delta T = 2$ °C), upon a sudden decrease from the isotropic temperature to 40.9 °C (0.2 °C above the BPI – BPII transition), the BPII<sub>(100)</sub> is nucleated mainly from the chemically patterned surface. As expected, since the gap between the patterned areas is lower than the correlation length ( $w_h < w_g$ ), the BPII<sub>(100)</sub> grows outside of each of the patterned regions up the point where it connects with other BPII<sub>(100)</sub> crystals that come from neighboring patterned regions. After 5 minutes, a BPII<sub>(100)</sub> single crystal is formed over the whole 440 x 440  $\mu\text{m}$  area. In addition to the blue color, the Kossel diagram confirms

the (100)-lattice orientation of the BPII.

Figure 3b shows the formation of BPII structures over long-type chemical patterns under two quench steps (each step is  $\Delta T=1^\circ\text{C}$ ), i.e. a sudden decrease to  $41.9^\circ\text{C}$  followed by a decrease of  $1^\circ\text{C}$  after 1 minute. When the temperature drops from the isotropic temperature to  $41.9^\circ\text{C}$ ,  $\text{BPII}_{(100)}$  starts to nucleate on the chemically-patterned area. However, a competition arises between the patterned area, the non-patterned area, and the top substrate. The BPII turns out to be polycrystalline, consisting of multiple domains oriented in different directions. By quenching the system another  $1^\circ\text{C}$ , the remaining  $\text{BPII}_{(100)}$  domains grow with time. In contrast to the fast cooling scheme, a uniform  $\text{BPII}_{(100)}$  cannot be achieved over the  $440 \times 440 \mu\text{m}$  area by means of an intermediate cooling rate. The slower cooling rate allows the nucleation of BPII domains with different lattice orientations in the bulk and at the top surface, which leads to the observed polycrystalline texture.

Under the slow cooling process ( $0.4^\circ\text{C} / \text{min}$ ) (Fig. 3c), the nucleation of a few randomly distributed  $\text{BPII}_{(100)}$  grains can be observed. At the quench step, the chemical patterns strongly dominate the formation of  $\text{BPII}_{(100)}$ . However, a surface mediated mechanism from both the top surface and the non-patterned area contribute to favor the  $\text{BPII}_{(111)}$  orientation, resulting in multiple domains aligned in different directions.

BPII formations on the short-type pattern ( $w_p = 10 \mu\text{m}$ ,  $w_h = 5 \mu\text{m}$ ) are also examined under the same cooling processes (fast, intermediate, and slow cooling), and show a similar behavior for nucleation and growth as that observed on the long-type pattern (Figure S1 in Supporting Information).

### **BP crystal nucleation and growth on reduced pattern surfaces from a cholesteric phase**

The growth of  $\text{BPII}_{(100)}$  single crystals are examined during heating from the cholesteric phase. Figure 4a shows several representative POM images of the phase behavior of the ChLC over the long type pattern when a fast heating rate ( $0.2^\circ\text{C} / \text{min}$ ) is used. At room temperature, the material is in the cholesteric phase, undergoing a transition to BPI at  $39.9^\circ\text{C}$ . Throughout the BPI regime, the  $\text{BPI}_{(110)}$  and  $\text{BPI}_{(200)}$  phases co-exist, resulting in a texture characterized by green and blue platelets, where the patterns are unable to direct the liquid crystalline self-assembly to produce a BPI single-crystal. At the BPI–BPII transition, spontaneous  $\text{BPII}_{(100)}$

crystal nucleation and growth occurs over the chemically-patterned areas, leading to a uniform  $\text{BPII}_{(100)}$  single-crystal that is maintained until the temperature is close to the isotropic temperature. As a comparison, the formation of BP structures above the short-type pattern under the same heating process is shown in Figure 4b, with a similar trend. A noteworthy feature here is that the  $\text{BPII}_{(100)}$  crystal that grew from the chemical patterns could not merge at the BPI–BPII transition, in contrast to what is observed for the  $\text{BPII}_{(100)}$  formation over the long-type pattern. Here, the  $\text{BPII}_{(100)}$  crystal requires a few minutes (c. 3 minutes) to fully merge over both chemically-patterned and non-patterned areas, and it remains unchanged until the system reaches the isotropic phase. The dependency of the  $\text{BPII}_{(100)}$  coarsening with respect to the chemical pattern type is related to the different correlation lengths; for the long-type pattern, this length is twice as large as that corresponding to the short-type pattern, leading to a different behavior at the BPI–BPII transition.

By analogy to the  $\text{BPII}_{(100)}$  single-crystal formation achieved with a fast heating rate, when a slow heating rate ( $0.04\text{ }^\circ\text{C} / \text{min}$ ) is used, a uniform  $\text{BPII}_{(100)}$  single crystal starts to grow once the liquid crystal reaches the BPI–BPII transition temperature for both long- and short-type pattern (Figure S2a and S2b). In contrast to the  $\text{BPII}_{(100)}$  single-crystal formation obtained by a cooling process, during heating the BPI structure plays an important role in forming  $\text{BPII}_{(100)}$  crystals, since the latter are generated from BPI crystals through a diffusion-less martensitic-like process<sup>29</sup>. Such a process is responsible for spontaneous  $\text{BPII}_{(100)}$  single-crystal formation.

### **Variation of the width of homeotropic anchoring region**

To better understand the influence of the width ( $w_h$ ) of the homeotropic anchoring region, we study the cases when  $w_h$  varies from 2 to 20  $\mu\text{m}$  for a fixed chemical pattern area ( $w_p = 10\text{ }\mu\text{m}$ ), which corresponds to the minimum width for which a whole-area single crystal can be obtained. Figure 5a shows BPII formation over the long-type pattern obtained by a fast cooling rate ( $2\text{ }^\circ\text{C} / \text{min}$ ). Fully coarsened  $\text{BPII}_{(100)}$  is observed when  $w_h$  is below 10  $\mu\text{m}$ . The  $\text{BPII}_{(100)}$  crystal coarsens within 30 seconds when the space between chemical patterns is  $w_h = 2\text{ }\mu\text{m}$ . As  $w_h$  increases, more time is needed to bridge the  $\text{BPII}_{(100)}$  domains that grow from the chemical-patterned areas. Surprisingly, a  $\text{BPII}_{(100)}$  single crystal is not achieved when the  $w_h$  is wider than 15  $\mu\text{m}$ . Despite the fact that the  $\text{BPII}_{(100)}$ -correlation length is  $11\pm 1\text{ }\mu\text{m}$ , we observed a polycrystalline structure when using the long type pattern.

The  $\text{BPII}_{(100)}$  coarsening from the short type patterns shows similar behavior (Figure 5b). When  $w_h$  is small, each  $\text{BPII}_{(100)}$  formed on the chemical patterns grows and covers both chemically-patterned areas and homeotropic anchoring spaces. Notably, more time is required to coarsen the  $\text{BPII}_{(100)}$  domains; for example, a fully merged  $\text{BPII}_{(100)}$  is obtained after one minute when  $w_h$  is 2  $\mu\text{m}$ . The growth rate of the  $\text{BPII}_{(100)}$  over short type patterns is slower than that measured over long type patterns, where a few more minutes are needed to obtain full a  $\text{BPII}_{(100)}$  crystal. When  $w_h$  is larger than 15  $\mu\text{m}$ ,  $\text{BPII}_{(111)}$  grains are formed and remain stable. When  $w_h$  is 20  $\mu\text{m}$ , the  $\text{BPII}_{(100)}$  domains are only located on the chemically-patterned areas. The correlation length of the  $\text{BPII}_{(100)}$  from short-type patterns is  $7 \pm 1 \mu\text{m}$ , which is significantly shorter than that obtained on long-type patterns.

Taken together, our findings indicate that the correlation lengths for long- and short-type patterns behave differently. In addition, when considering homeotropic gap widths between the patterned sections slightly lower than the correlation length, we find that such a gap is not sufficient to guarantee the formation of a single  $\text{BPII}_{(100)}$  crystal. We can interpret these observations in terms of competition between substrate-induced and grain-boundary contributions to the total free energy of the system, as shown in Figure 6.

Firstly, consider the free-energy difference per unit area ( $A$ ) between the heterogeneous state with  $\text{BPII}_{(100)}$  covering a patterned region of width  $w_p$  (and  $\text{BPII}_{(111)}$  covering the un-patterned substrate) with the homogeneous state where the entire surface is covered with  $\text{BPII}_{(111)}$  (shown schematically in Fig. 6),

$$\frac{\Delta F(w_p)}{A} = - \left[ f_{\frac{111}{p}} - f_{\frac{100}{p}} \right] w_p + 2\gamma_{up}$$

where  $f_{\frac{o}{s}}$  represents the substrate-induced free-energy density of orientation  $o = (100)$  or  $(111)$  covering substrate  $s = p$  or  $u$ , while  $\gamma_{up}$  represents the grain-boundary free-energy density associated with the interface between  $\text{BPII}_{(111)}$  over  $u$  and  $\text{BPII}_{(100)}$  over  $p$ . Since  $(100)$  is more stable than  $(111)$  over the patterned region,  $\Delta f_p \equiv f_{\frac{111}{p}} - f_{\frac{100}{p}} > 0$ . The heterogeneous state is stable only when  $\frac{\Delta F(w_p)}{A} < 0$ , which occurs for

$$w_p > w_p^{\min} = 2 \frac{\gamma_{up}}{\Delta f_p}$$

From this expression, we arrive at an estimate for  $\gamma_{up}$ . Using the value  $\Delta f_p \sim 1 \text{ Jm}^{-3}$  (obtained from simulations<sup>21</sup>) and the measured value  $w_p^{\min} \sim 10 \text{ }\mu\text{m}$ , we estimate  $\gamma_{up} \sim 10^{-6}$  to  $10^{-5} \text{ Jm}^{-2}$ . Knowing  $\gamma_{up}$  we can calculate an effective elastic constant associated with gradients of orientation in BPs. Assuming that such changes occur over distances on the order of the unit-cell size,  $\Delta x = 100 \text{ nm}$ , the grain-boundary free-energy density would be  $\gamma \sim K/\Delta x$ . Solving for the elastic constant we arrive at  $K \sim 10^{-12} \text{ N}$ , which is comparable to the elastic constants of low-molecular-weight thermotropic materials<sup>32</sup>. In addition, our observation that  $w_p^{\min}$  is larger for the long than for the short-type pattern can be interpreted as arising from different values of the grain-boundary free-energy density  $\gamma_{up}$ : the two orientations (100) and (111) meet over the smooth boundary adjacent to the long axis of the chemical stripes in the first case, and over a more irregular collection of chemical stripe tips in the second case.

To find the maximum width  $w_g^{\max}$  that  $\text{BPII}_{(100)}$  can protrude into the un-patterned region, consider the free energy difference between the protruded and non-protruded heterogenous states shown in Fig. 6. Assuming by symmetry the same protrusion on both sides of the patterned region, we now have

$$\frac{\Delta F(w_g)}{A} = 2 \left[ f_{\frac{100}{u}} - f_{\frac{111}{u}} \right] w_g + 2[\gamma_{uu} - \gamma_{up}].$$

Orientation (111) is more stable over the un-patterned region, so  $\Delta f_u \equiv f_{\frac{100}{u}} - f_{\frac{111}{u}} > 0$ . The protruded state can only be stable when the grain-boundary free-energy density  $\gamma_{uu}$  (of orientations (111) and (100) meeting over  $u$ ) satisfies  $\gamma_{uu} < \gamma_{up}$  and

$$w_g < w_g^{\max} = \frac{\gamma_{up} - \gamma_{uu}}{\Delta f_u}.$$

The requirement  $\gamma_{uu} > 0$  leads to the condition  $\frac{\Delta f_p}{\Delta f_u} > \frac{2w_g^{\max}}{w_p^{\min}}$ . From the measured values  $w_p^{\min} = 10 \text{ }\mu\text{m}$  and  $w_g^{\max} = (11 \pm 1) \text{ }\mu\text{m}$ , we obtain  $\frac{\Delta f_p}{\Delta f_u} = 2.2 \pm 0.2$ .

Finally, to analyze the maximum width  $w_h^{\max}$  of unpatterned substrate that  $\text{BPII}_{(100)}$  can span

while covering uniformly the whole surface (see Fig. 6), consider the free energy difference between such homogenous state and the protruded state with  $w_g = w_g^{max}$ ,

$$\frac{\Delta F(w_h)}{A} = 2 \left[ f_{\frac{100}{u}} - f_{\frac{111}{u}} \right] (w_h - 2w_g^{max}) - 2\gamma_{uu}.$$

Now, the homogenous  $\text{BPII}_{(100)}$  state is stable only for

$$w_h < w_h^{max} = \frac{2\gamma_{uu}}{\Delta f_u} + 2w_g^{max} = w_p^{min} \frac{\Delta f_p}{\Delta f_u}.$$

Since this expression depends on the ratio of substrate-induced free-energy differences, our previous results predict  $w_h^{max (predicted)} = 22 \pm 2 \mu\text{m}$ . The measured value  $w_h^{max (measured)} = 15.0 \pm 2.5 \mu\text{m}$  is below the predicted limit. It is of interest to point out that this limit depends on the ratio of  $\Delta f_p$  and  $\Delta f_u$  as opposed to their absolute values. In summary of our theoretical calculations, heterogenous states can be stable if the most stable phase over a given substrate advances sufficiently to compensate for the presence of grain boundaries. Thus, competition between thermodynamically favorable interaction between one or other phase over a given substrate can drive or limit the observation of homogeneous states and determine the maximum protrusion and gap-bridging distances.

## Conclusion

In summary, we have characterized and analyzed the critical nucleation dimensions, crystal growth dynamics, and correlation length of  $\text{BPII}_{(100)}$  assisted by designed binary chemically-patterned surfaces.  $\text{BPII}_{(100)}$  single crystals are formed over the chemically-patterned areas and start to propagate into the surrounding non-patterned regions. A successful  $\text{BPII}$ -crystal nucleation and growth, that ends in a  $\text{BPII}_{(100)}$  single-crystal, is possible when the patterned region has lateral dimensions above  $10 \mu\text{m}$ . The  $\text{BPII}$ -correlation length was found to be dependent on the crystal growth time and the characteristics of the chemical pattern. This length keeps a consistent value of the order of  $10 \mu\text{m}$  which is in accordance to the minimum lateral dimensions needed for a patterned area to achieve a defect-free  $\text{BPII}$  single crystal. Uniform coarsening can be completed by different kinetic pathways, including fast cooling and heating processes. The spaces between chemical patterns affect the  $\text{BPII}_{(100)}$  coarsening, specifically

for  $w_h > 15 - 20 \mu\text{m}$  other BPII orientations become stable between the chemically-patterned areas. This work demonstrates the ability of using reduced chemical pattern or partial patterned areas for stabilizing large areas 3D soft liquid crystalline structures, which will facilitate the future design strategies to produce large-scale single-crystal BPs for exploration and development of BPLC-based electro-optical devices.

### **Experimental Section:**

**Preparation of materials:** BP material consists of MLC 2142 and 4-(1-methylheptyloxycarbonyl)phenyl-4-hexyloxybenzoate (S-811, 36.32 wt%) purchased from Merck. Toluene was used as a cosolvent to mix MLC 2142 and S-811, then evaporated under vacuum at 55 °C overnight. All the other chemicals and solvents were purchased from Sigma-Aldrich and used without further purification.

**Preparation of chemical patterns:** A ~4 nm PMMAZO (poly(6-(4-methoxy-azobenzene-4'-oxy) hexyl methacrylate)) thin film was prepared by spin-coating 0.05 wt% PMMAZO solution on piranha solution cleaned silicon substrate, and annealing at 250 °C for 5 min under N<sub>2</sub>. The un-grafted PMMAZO was washed away by sonicating the substrate in chlorobenzene for three times and each time 5 min. Electron beam lithography process was performed using JEOL 9300FS at the Center for Nanoscale Materials, Argonne National Lab. Stripe patterns of different designs were exposed on the photoresist layer and transformed into chemical patterns on the PMMAZO brush layer using O<sub>2</sub> plasma etching, followed by stripping the photoresist in chlorobenzene.

**Preparation of LC cell:** Octadecyltrichlorosilane modified glass slides was used as top surface to assemble face-to-face with a patterned PMMAZO substrate. A 3.5 μm Myler film was used as space to separate two surfaces. The BP material was heated above the isotropic transition temperature, and injected into the heated LC cell by capillary action. The system was then slowly cooled down to room temperature.

**Characterization:** The chemical pattern on PMMAZO brush layer were inspected with Scanning electron microscopy (SEM, ZEISS MERLIN). The optical images of the LC cell were obtained with a BX 60 Olympus polarized light microscope equipped with Bertrand lens and 405 nm monochromic light filter. The Linkam PE120 heating stage was used to control the

thermal process on BP sample at different heating/cooling rates. Kossel diagram was used to determine the phase and crystal orientation.

The detailed information of materials, sample preparation and characterization are available in refs 29 and 30.

### **Figures and Captions:**

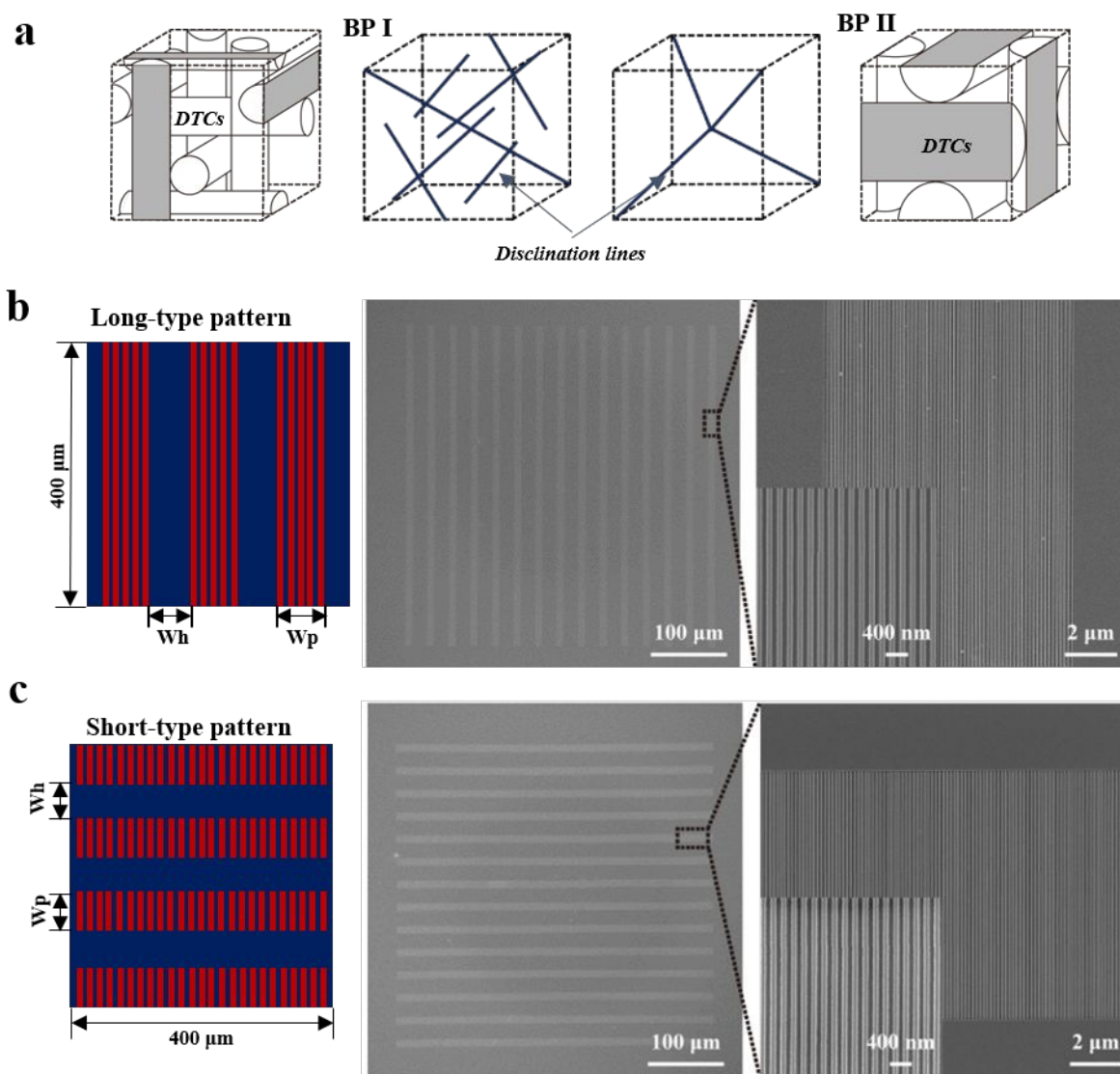


**Figure 1.** a) Unit cell structures and disclination lines for BPI and BPII. Two different chemical pattern designs and corresponding SEM images: b) long-type pattern, and c) short-type pattern (planar:  $\sim 75$  nm width / homeotropic:  $\sim 75$  nm width).

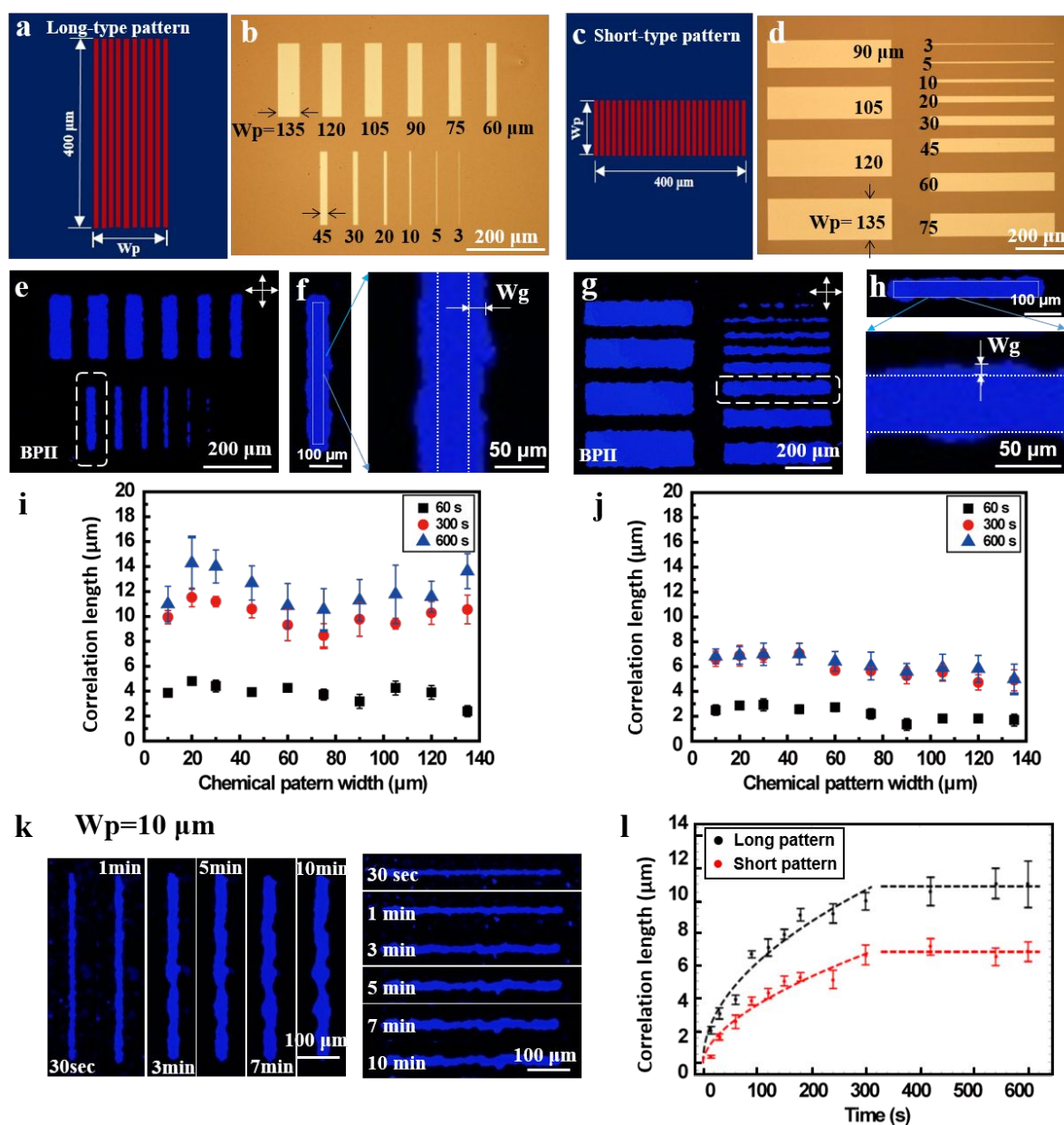


**Figure 2.** Design of a) the long-type chemical pattern and c) the short-type chemical pattern, and b, d) reflection OM images of chemically-patterned areas of a variety of widths ( $w_p = 3 - 135 \mu\text{m}$ ). e, g) Reflection POM images of BPII at  $41.9 \text{ }^\circ\text{C}$  upon cooling and f, h) the correlation length of  $\text{BPII}_{(100)}$  measured from the chemical patterns ( $w_p = 45 \mu\text{m}$ ). i, j) The correlation length  $w_g$  of  $\text{BPII}_{(100)}$  as a function of the width of chemical pattern area and time. k) Reflection POM images and l) the correlation length of  $\text{BPII}_{(100)}$  measured from the chemical pattern ( $w_p$

= 10  $\mu\text{m}$ ) at different times; two processes can be resolved: a short-time process with a power-law exponent  $n=1/2$ , followed by a constant-value one.

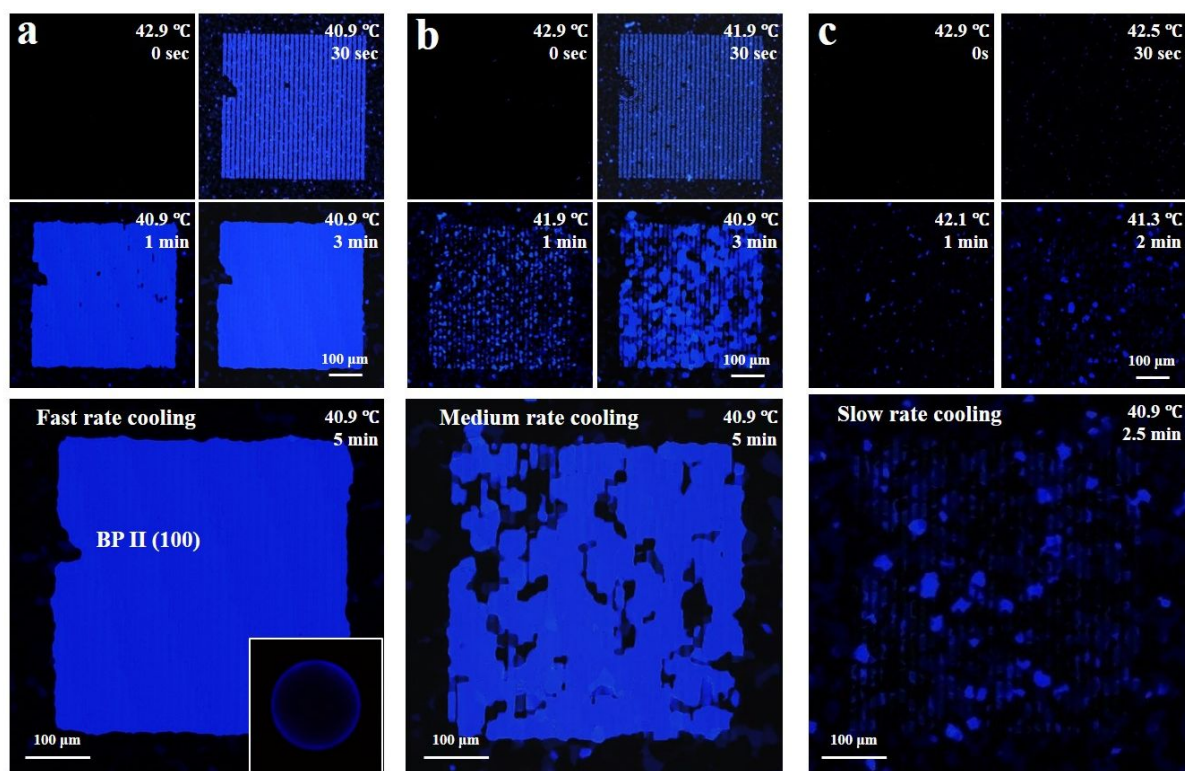


**Figure 3.** Reflection POM images of BP II<sub>(100)</sub> on the long-type chemical pattern ( $w_p = 10 \mu\text{m}$ ,  $w_h = 5 \mu\text{m}$ ) according to different cooling processes: a) fast cooling, b) medium cooling, and c) slow cooling.

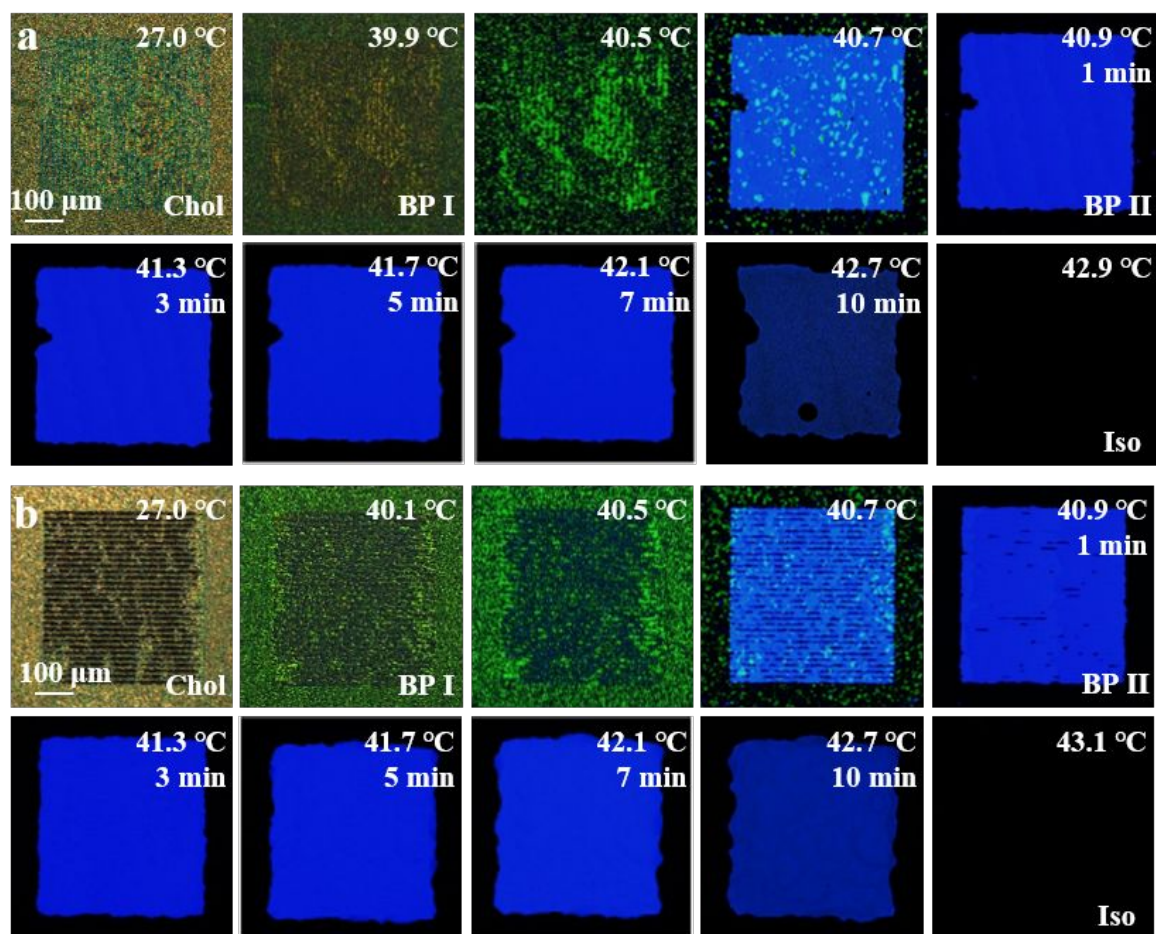


**Figure 4.** Reflection POM images of BP transition by fast heating ( $0.2\text{ }^{\circ}\text{C} / \text{min}$ ) process on a) long-type pattern and b) short-type pattern, with  $w_p = 10\text{ }\mu\text{m}$ ,  $w_h = 5\text{ }\mu\text{m}$ .

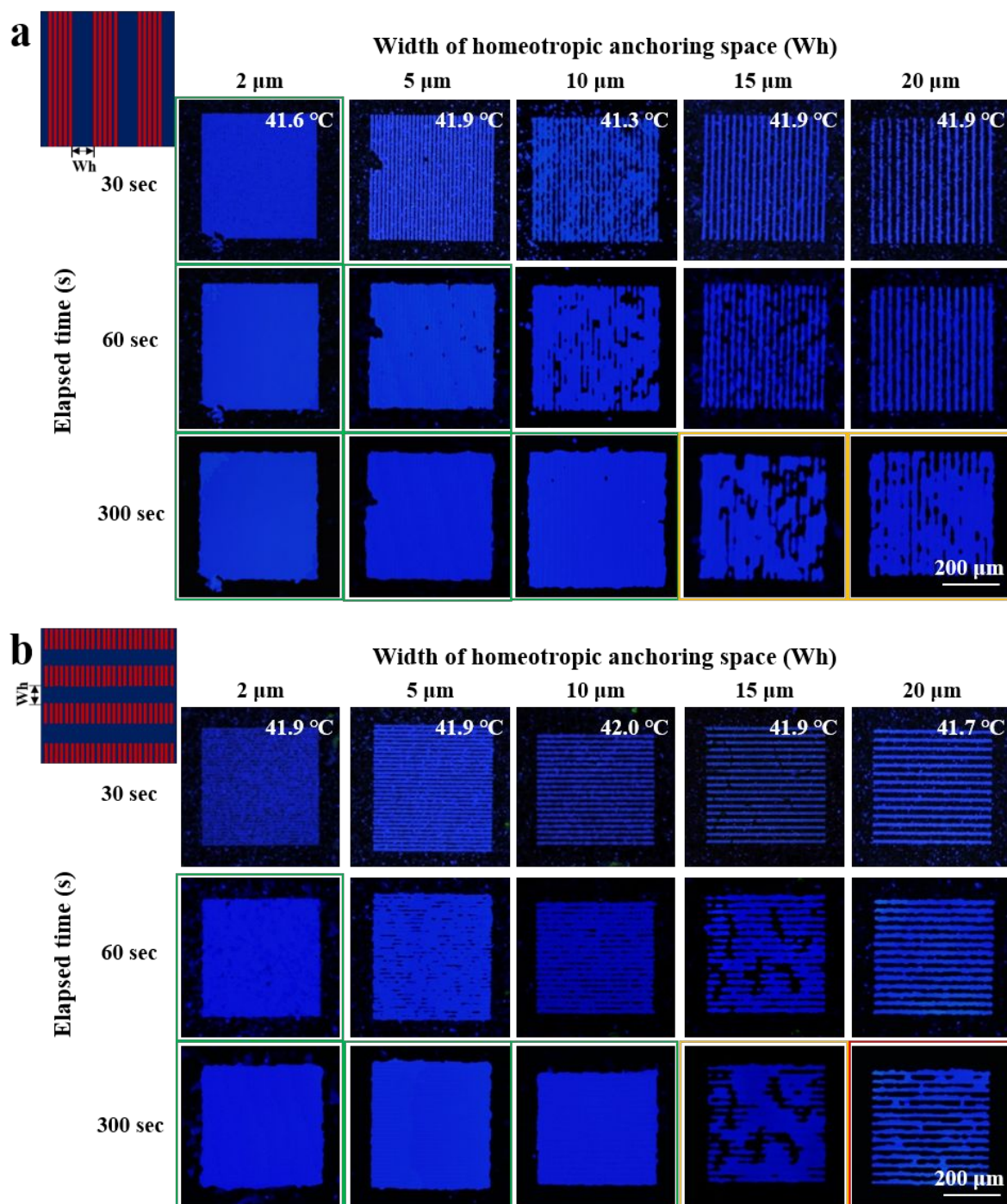


**Figure 5.** Reflection POM images of BPII for a) long-type chemical pattern ( $w_p = 10 \mu\text{m}$ ) and b) short-type chemical pattern ( $w_p = 10 \mu\text{m}$ ) as a function of the width ( $w_h$ ) of the homeotropic anchoring gaps between chemically-patterned regions. Fast cooling rate ( $2 \text{ }^\circ\text{C} / \text{min}$ ) from isotropic phase to BPII progression.

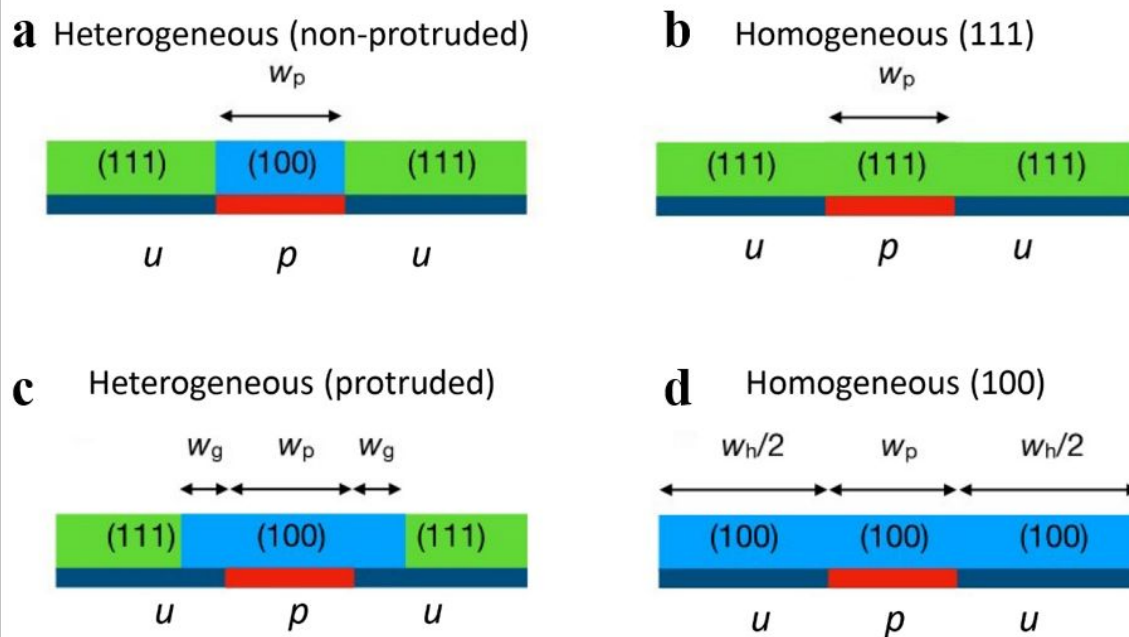


**Figure 6.** The stability condition of the heterogeneous (non-protruded) configuration (a) was obtained by comparing its free energy with that of the homogeneous (111) state (b) in terms of the width  $w_p$  of the patterned region. To find the maximum width  $w_g$  of a (100) protrusion over the un-patterned region  $u$ , the free energy of the heterogeneous (protruded) state (c) was compared with that of the heterogeneous (non-protruded) state (a). Finally, the maximum width  $w_h$  of the un-patterned region that can be spanned by  $BPII_{(100)}$  was found by comparing the free energy of the homogeneous (100) state (d) with that of the heterogeneous (protruded) state (c). In our analysis, we assume periodic boundary conditions for each of these four configurations.

## AUTHOR INFORMATION

### Corresponding Author

\*E-mail: Xiao.Li@unt.edu

\*E-mail: nealey@uchicago.edu

### Author contributions

X.L. and P.F.N. conceived and designed the experiments. X.L. and K.P. performed the experiments. J.A.M-G., O.G. and J.J. de. P. conceived and performed the theoretical calculations. X.L., K.P., J.A.M-G., O. G., J.A.D., J.J.de.P. and P.F.N. wrote the manuscript. X.L. and P.F.N. guided the work. All authors discussed the results and contributed to data analysis and manuscript revision.

## ACKNOWLEDGMENT

We gratefully acknowledge support by the U.S. Department of Energy, Basic Energy Sciences, Materials Sciences and Engineering Division. We acknowledge the use of the facility resources provided by the Center for Nanoscale Materials, a U. S. Department of Energy (DOE) Office of Science User Facility operated for the DOE Office of Science by Argonne National Laboratory under Contract No. DE-AC02-06CH11357, and the University of Chicago MRSEC Shared User Facilities (NSF DMR-1420709). JAMG gratefully acknowledges support by the Laboratorio Nacional de Supercomputo del (LNS) a member of CONACYT national laboratories, with project number No. 201901023N.

## References

1. Wright, D. C.; Mermin, N. D. Crystalline Liquids - the Blue Phases. *Rev. Mod. Phys.* **1989**, 61 (2), 385-432.
2. Seideman, T. The Liquid-Crystalline Blue Phases. *Rep. Prog. Phys.* **1990**, 53 (6), 659-705.
3. Kikuchi, H. Liquid crystalline blue phases. *Struct. Bond.* **2008**, 128, 99-117.
4. Rahman, M. D. A.; Said, S. M.; Balamurugan, S. Blue phase liquid crystal: strategies for phase stabilization and device development. *Sci. Technol. Adv. Mat.* **2015**, 16 (3).
5. Gandhi, S.S.; Kim, M.S.; Hwang, J.-Y.; Chien, L.-C. Electro-optical Memory of a Nanoengineered Amorphous Blue-Phase III Polymer Scaffold. *Adv. Mater.* **2016**, 28, 8998-9005.
6. Henrich, O.; Stratford, K.; Cates, M.E.; Marenduzzo, D. Structure of Blue-Phase III of Cholesteric Liquid Crystals. *Phys. Rev. Lett.* **2011**, 106, 107801.
7. Cao, W. Y.; Munoz, A.; Palffy-Muhoray, P.; Taheri, B. Lasing in a three-dimensional photonic crystal of the liquid crystal blue phase II. *Nat. Mater.* **2002**, 1 (2), 111-113.
8. Lin, T. H.; Li, Y. N.; Wang, C. T.; Jau, H. C.; Chen, C. W.; Li, C. C.; Bisoyi, H. K.; Bunning, T. J.; Li, Q. Red, Green and Blue Reflections Enabled in an Optically Tunable Self-Organized 3D Cubic Nanostructured Thin Film. *Adv. Mater.* **2013**, 25 (36), 5050-5054.
9. Zheng, Z.-G.; Yuan, C.-L.; Hu, W.; Bisoyi, H. K.; Tang, M.-J.; Liu, Z.; Sun, P.-Z.; Yang, W.-Q.; Wang, X.-Q.; Shen, D.; Li, Y.; Ye, F.; Lu, Y.-Q.; Li, G.; Li, Q. Light patterned crystallographic direction of a self-organized 3D soft photonic crystal. *Adv. Mater.* **2017**, 29, 1703165.
10. Lu, S. Y.; Chien, L. C. Electrically switched color with polymer-stabilized blue-phase liquid crystals. *Opt. Lett.* **2010**, 35 (4), 562-564.
11. Yan, J.; Wu, S. T.; Cheng, K. L.; Shiu, J. W. A full-color reflective display using polymer-stabilized blue phase liquid crystal. *Appl. Phys. Lett.* **2013**, 102 (8).
12. Xiang, J.; Lavrentovich, O. D., Blue-phase-polymer-templated nematic with sub-millisecond broad-temperature range electro-optic switching. *Appl. Phys. Lett.* **2013**, 103 (5).
13. Castles, F.; Morris, S. M.; Hung, J. M. C.; Qasim, M. M.; Wright, A. D.; Nosheen, S.; Choi, S. S.; Outram, B. I.; Elston, S. J.; Burgess, C.; Hill, L.; Wilkinson, T. D.; Coles, H. J. Stretchable liquid-crystal blue-phase gels. *Nat. Mater.* **2014**, 13 (8), 817-821.
14. Jo, S. Y.; Jeon, S. W.; Kim, B. C.; Bae, J. H.; Araoka, F.; Choi, S. W., Polymer Stabilization

- of Liquid-Crystal Blue Phase II toward Photonic Crystals. *ACS Appl. Mater. Inter.* **2017**, *9* (10), 8941-8947.
15. Nayek, P.; Jeong, H.; Park, H. R.; Kang, S. W.; Lee, S. H.; Park, H. S.; Lee, H. J.; Kim, H. S., Tailoring Monodomain in Blue Phase Liquid Crystal by Surface Pinning Effect. *Appl. Phys. Express* **2012**, *5* (5).
16. Joshi, P.; Shang, X. B.; De Smet, J.; Islamai, E.; Cuypers, D.; Van Steenberghe, G.; Van Vlierberghe, S.; Dubruel, P.; De Smet, H. On the effect of alignment layers on blue phase liquid crystals. *Appl. Phys. Lett.* **2015**, *106* (10).
17. Chen, P. J.; Chen, M.; Ni, S. Y.; Chen, H. S.; Lin, Y. H. Influence of alignment layers on crystal growth of polymer-stabilized blue phase liquid crystals. *Opt. Mater. Express* **2016**, *6* (4), 1003-1010.
18. Chen, Y.; Wu, S. T. Electric field-induced monodomain blue phase liquid crystals. *Appl. Phys. Lett.* **2013**, *102* (17).
19. Li, W. H.; Hu, D. C.; Li, Y.; Chen, C. P.; Lee, Y. J.; Lien, A.; Lu, J. G.; Su, Y. K. Fringing field-induced monodomain of a polymer-stabilized blue phase liquid crystal. *Appl. Phys. Lett.* **2015**, *107* (24).
20. Nayek, P.; Park, N. H.; Noh, S. C.; Lee, S. H.; Park, H. S.; Lee, H. J.; Hou, C. T.; Lin, T. H.; Yokoyama, H. Analysis of surface anchored lattice plane orientation in blue phase liquid crystal and its in-plane electric field-dependent capacitance response. *Liq. Cryst.* **2015**, *42* (8), 1111-1119.
21. Martinez-Gonzalez, J. A.; Li, X.; Sadati, M.; Zhou, Y.; Zhang, R.; Nealey, P. F.; de Pablo, J. J. Directed self-assembly of liquid crystalline blue-phases into ideal single-crystals. *Nat. Commun.* **2017**, *8*, 15854.
22. Li, X.; Martinez-Gonzalez, J. A.; Park, K.; Yu, C.; Zhou, Y.; de Pablo, J. J.; Nealey, P. F. Perfection in Nucleation and Growth of Blue-Phase Single Crystals: Small Free-Energy Required to Self-Assemble at Specific Lattice Orientation. *ACS Appl. Mater. Interfaces.* **2019**, *11*, 9487-9495.
23. Li, X.; Martinez-Gonzalez, J. A.; Guzman, O.; Ma, X.; Park, K.; Jin, H. M.; Dolan, J.; Nealey, P. F.; de Pablo, J. J. Sculpted Grain Boundaries in Soft Crystals. *Sci. Adv.* **2019**, *5*, eaax9112.
24. Diekmann, K.; Schumacher, M.; Stegemeyer, H. Nucleus growth in liquid crystals. *Liq. Cryst.* **1998**, *25* (3), 349-355.
25. Dierking, I. Domain growth scaling at the isotropic-to-cholesteric liquid crystal transition. *J. Phys. Chem. B* **2000**, *104* (45), 10642-10646.
26. Demikhov, E.; Stegemeyer, H.; Blumel, T. Domain Growth Laws for the Phase Ordering of Chiral Liquid-Crystals. *Phys. Rev. E* **1994**, *49* (6), R4787-R4790.
27. Schumacher, M.; Demikhov, E.; Stegemeyer, H. Phase ordering kinetics in chiral liquid crystals. *Mol. Cryst. Liq. Cryst. A* **1995**, *260*, 395-&.
28. Dierking, I. Universal growth laws in liquid crystals far from equilibrium. *Appl. Phys. a-Mater.* **2001**, *72* (3), 307-310.
29. Li, X.; Martinez-Gonzalez, J. A.; Hernandez-Ortiz J. P., Ramirez-Hernandez A., Zhou Y., Sadati M., Zhang R., Nealey P. F., de Pablo J. J. Mesoscale Martensitic Transformation in Single Crystals of Topological Defects. *PNAS*, **2017**, *114*, 10011-10016.
30. Li, X.; Armas-Perez, J. C.; Martinez-Gonzalez, J. A.; Liu, X. Y.; Xie, H. L.; Bishop, C.;

Hernandez-Ortiz, J. P.; Zhang, R.; de Pablo, J. J.; Nealey, P. F. Directed self-assembly of nematic liquid crystals on chemically patterned surfaces: morphological states and transitions. *Soft Matter* **2016**, 12 (41), 8595-8605.

31. Bray, A.J. Theory of Phase-ordering kinetics. *Adv. Phys.* **1994**, 43, 357-459.

32. de Gennes, P. G.; Prost, J. *The Physics of Liquid Crystals*. 2<sup>nd</sup> ed, Oxford UP. **1993**.